Available online at www.sciencedirect.com
SCIENCE DIRECT®
Physics of the Earth and Planetary Interiors xxx (2004) xxx–xxx
PHYSICS OF THE EARTH AND PLANETARY INTERIORS
www.elsevier.com/locate/pepi

Group-velocity tomography and lithospheric S-velocity structure of the South American continent

Mei Feng[a], Marcelo Assumpção[a,*], Suzan Van der Lee[b,1]

[a] *Department of Geophysics, IAG, University of São Paulo, Rua do Matão 1226, São Paulo, SP 05508-090, Brazil*
[b] *ETH, Honggerberg, CH-8093, Zurich, Switzerland*

Received 4 March 2004; received in revised form 12 May 2004; accepted 14 July 2004

Abstract

The lithosphere of the South American continent has been studied little, especially in northern Brazil (the Amazonian region). A 3D lithospheric S-velocity model of South America was obtained by first carrying out Rayleigh and Love wave group-velocity tomography, and then inverting the regionalized dispersion curves. Fundamental mode group velocities were measured using a Multiple Filtering Technique. More than 12,000 paths were examined and about 6000 Rayleigh- and 3500 Love-wave dispersion curves with good quality were retrieved. Checkerboard tests showed that our dataset permits the resolution of features 400–800 km across laterally in the central part of the continent from crustal to upper mantle depths. Our results confirm previous tomographic results and correlate well with the major geological provinces of South America. The 3D S-velocity model confirms both regional features of SE Brazil from P-wave travel-time tomography and continental-scale features of central and western South America from waveform inversion, e.g., lowest velocities in the Andean upper mantle; three parts of the Nazca plate with flat subduction; strong low-velocity anomalies in the upper-mantle depth beneath the Chaco basin. Furthermore, our 3D model revealed new features in the South American continent: (1) high velocities in the lower crust were consistently found in regions with high Bouguer or free-air anomalies; (2) the NE–SW trending TransBrasiliano shear zone was delineated by a NE–SW low-velocity belt at lithospheric depths; (3) the eastern Amazonian craton appears to have thicker lithosphere than the western craton; (4) in areas of Archean nuclei located in the northeastern Guaporé shield and southeastern São Francisco craton, high velocity anomalies were found down to 150 km.

Keywords: Surface wave tomography; Group-velocity; Lithosphere; S-velocity; South American continent

1. Introduction

The lithospheric structure of the South American platform is still poorly known because of the sparse seismic station distribution. Fig. 1 shows the main South American geological provinces discussed in this

* Corresponding author. Fax: +55 11 30915034.
E-mail addresses: mei@iag.usp.br (M. Feng), marcelo@iag.usp.br (M. Assumpção), suzan@earth.northwestern.edu (S. Van der Lee).
[1] Present address: Northwestern University, 1850 Campus Drive, Evanston, IL 60208, USA.

0031-9201/$ – see front matter © 2004 Elsevier B.V. All rights reserved.
doi:10.1016/j.pepi.2004.07.008

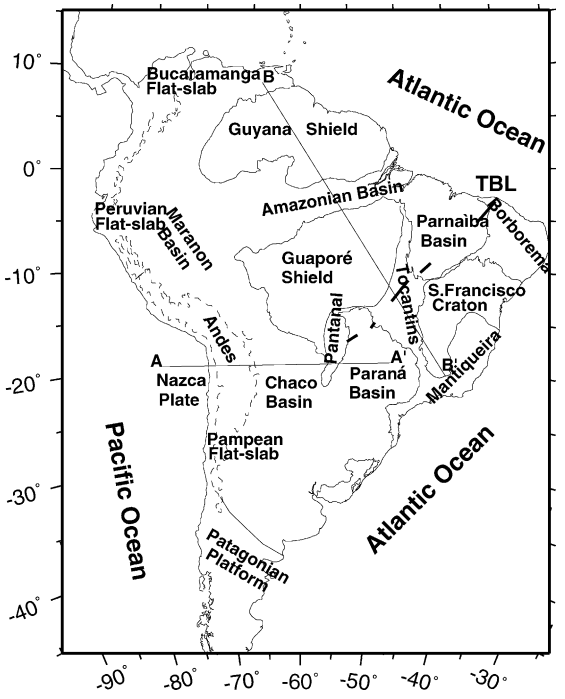

Fig. 1. Schematic map of South America with the main geological and tectonic provinces. AA′ and BB′ are two profiles discussed later in this study. TBL indicates the TransBrasiliano Lineament.

work. The upper mantle in the Andean region has been studied with P- and S-wave velocity or attenuation tomography (e.g., Engdahl et al., 1995; Myers et al., 1998; Dorbath and Masson, 2000; Haberland and Rietbrock, 2001) to characterize the Nazca slab and the asthenospheric wedge. In a small area of Southeast Brazil, around the northern part of the Paraná Basin, P- and S-wave travel-time tomography are beginning to map upper mantle structures (VanDecar et al., 1995; Schimmel et al., 2003; Assumpção et al., 2004). However, for most of the stable South American platform, sparse station distribution has prevented mapping upper mantle structure with adequate resolution. Compared with other continents, such as North America (e.g., Grand, 1994; Alsina et al., 1996; Van der Lee and Nolet, 1997; Godey et al., 2003; Nettles and Dziewonski, 2003), Eurasia (e.g., Snieder, 1988; Zielhuis and Nolet, 1994; Ritzwoller and Levshin, 1998; Villaseñor et al., 2001; Marone et al., 2003; Yanovskaya and Kozhevnikov, 2003), and Australia (e.g., Simons et al., 1999; Debayle and Kennett, 2000), the South American continent is still one of the least studied and the resolution of previous tomographic studies is still poor.

Inter-station phase velocities have been used only in a few isolated studies in Eastern South America, such as in the Atlantic shield (Souza, 1991) and the Paraná and Chaco basins (Snoke and James, 1997; Snoke and Sambridge, 2002; An and Assumpção, 2004). Regional surface wave tomography using long paths from the global permanent network (Silveira et al., 1998; Silveira and Stutzmann, 2002; Vdovin et al., 1999) have mapped features of the order of 1000–700 km. Global studies (Ekstrom and Dziewonski, 1998; Larson and Ekstrom, 2001; Boschi and Ekstrom, 2002; Ritzwoller et al., 2002; Shapiro and Ritzwoller, 2002) also have resolutions of the order of 1000 km for periods of 100–150 s or depths around 150 km.

A more detailed regional tomography using additional temporary stations in SE Brazil and paths mainly in western and central South America was carried out by Van der Lee et al. (2001, 2002) by processing 550 waveforms with the Partitioned Waveform Inversion method (Nolet, 1990; Van der Lee and Nolet, 1997). Van der Lee et al. (2001, 2002) constructed waveforms by summing at least the first 20 modes, producing a model with best resolution in upper mantle depths. This model provides the most extensive map to date of the hydrated mantle wedge beneath the Andes, mentioned above. Furthermore, the lithosphere beneath the Chaco and Pantanal basins was characterized by low velocities, and the western part of the Amazonian craton was defined by high velocities, but the northeastern part of the continent had no coverage at all. More recently, Heintz (2003) and Heintz et al. (2004) presented a 3D upper mantle S-velocity structure using both temporary Brazilian stations and the global network on a region including neighboring plates. She used up to 5850 surface wave paths and a waveform inversion method with fundamental mode of periods higher than 40 s and first higher mode, which cannot constrain shallow structure. Her model, with about 500 km of lateral resolution and 50 km of vertical resolution, showed high lithospheric velocities in the northeastern part of the Amazonian Craton. A low velocity anomaly was found beneath the Chaco basin, compatible with dispersion results (Snoke and James, 1997; Snoke and Sambridge, 2002) as well as the model of Van der Lee et al. (2001, 2002).

All the regional and global studies tend to agree on the large scale features. For example, at periods near

100–150 s, higher surface wave velocities are generally found north of 20°S in the stable platform; S-wave velocities obtained for depths of 100–200 km also indicate thicker lithosphere in the northern part of the continent, which comprises the Amazonian and São Francisco cratons. However, the regional and global studies cannot usually distinguish between the two cratons, and discrepancies between different models are common. For example, the highest velocities at 200 km depth (indicating deepest lithosphere) were found by Heintz (2003) in the eastern part of the Amazonian craton, in the Guaporé shield, whereas Ritzwoller et al. (2002) found the highest velocities in the western part of the craton, beneath the Amazon basin. Silveira and Stutzmann (2002) found low velocities beneath the Guyana shield and the western part of the Amazonian basin, at 200 km depth, opposite to the results of Shapiro and Ritzwoller (2002) and of Ritzwoller et al. (2002). These discrepancies are not only due to the use of different data sets and variable coverage but also to different inversion techniques. Ritzwoller et al. (2002) observe that diffraction tomography yields stronger velocity anomalies that extend deeper than great-circle based tomography used by Van der Lee et al., 2001; Silveira and Stutzmann, 2002; Shapiro and Ritzwoller, 2002; Heintz, 2003.

To improve the data coverage in South America, 15 new portable broadband stations (10 from ETH-Z, Switzerland, and 5 from USP, Brazil) have been deployed since 2002 in northern, northeastern and southernmost Brazil in a joint project between USP and ETH-Z, named Brazilian Lithosphere Seismic Project 2002 (BLSP02). We used the new temporary stations, together with the stations from previous BLSP projects (1992–2002) and the permanent GSN stations, with earthquakes mainly from the Andean region, to better map the first-order structure of the major lithospheric units of the South American continent.

Our inversion is carried out in two steps: (1) 2D group-velocity tomography and (2) 1D inversion of the regionalized dispersion curve to obtain the S-velocity profile of each cell. This two-step method of surface wave inversion for a 3D S-velocity model has been successfully applied in other regions (Ritzwoller and Levshin, 1998; Vuan et al., 2000; Villaseñor et al., 2001; Pasyanos et al., 2001; Huang et al., 2003; Yanovskaya and Kozhevnikov, 2003). With this

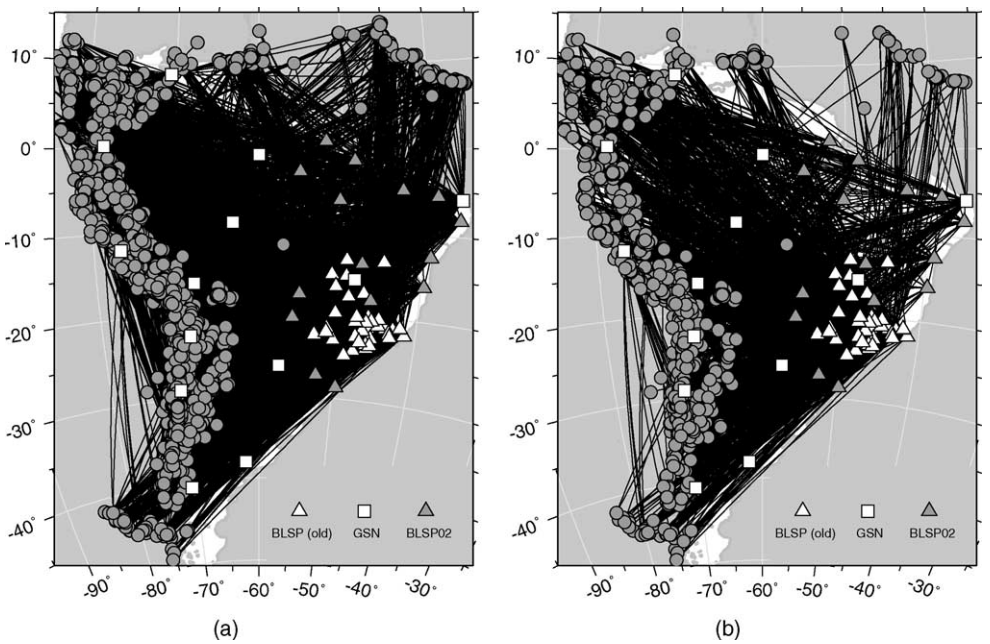

Fig. 2. Stations of BLSP projects (triangles) and GSN (squares), earthquakes (circles) and paths (black lines) used for Rayleigh (a) and Love (b) wave group-velocity tomography at 30 s period.

two-step method and the improved path coverage, high-resolution group-velocity maps and S-velocity lithospheric structures in the South American continent were determined.

We use a geometrical ray theory approximation because of its computational efficiency, rather than a diffraction tomography (Nolet and Dahlen, 2000; Spetzler et al., 2002; Ritzwoller et al., 2002; Yoshizawa and Kennett, 2002). Finite-frequency methods are likely important for very long paths and long periods where the Fresnel zone can be very wide. To minimize diffraction effects associated with long paths, we did not use earthquakes from the distant South Atlantic ridge or stations outside the continent. The restriction of using mainly purely continental paths also reduces refraction effects across the continent/ocean transition. Our data set indicates we can resolve features 400–800 km across laterally at depths from 30 to 150 km, as discussed later. We believe that our excellent path distribution (Fig. 2) tends to average out diffraction effects.

2. Main geological provinces in South America

The South American continent includes the seismically and magmatically active Andean chain in the west and north, the old stable Precambrian South American Platform in the center and east, and the Late Paleozoic Patagonian platform in the south (Ramos, 1999; Almeida et al., 2000). It is a tectonically complex region with large intracratonic sedimentary basins, Precambrian shields, fold belts and mountain ranges. A schematic map of the main geological units is shown in Fig. 1.

The Andean range is related to the Nazca plate subduction under the South American plate. The subduction geometry beneath the Andean cordillera shows along-strike variations in dip of the subducting Nazca plate from subhorizontal flat-slab segments to normal subduction (e.g., Cahill and Isacks, 1992; Ramos, 1999). Three flat-slab segments have been recognized along the Andes. From north to south, the first flat-slab segment is the Bucaramanga in the northern Andes north of 5°N (Pennington, 1981); the second is the Peruvian flat-slab segment between 5°S and 14°S (Cahill and Isacks, 1992; Ramos, 1999); the third one is the Pampean segment between 27°S and 33°S (Ramos, 1999). Between the Bucaramanga and Peruvian flat-slab segments (5°N–5°S), subduction is normal in Ecuador with a slab dip of about 35° (Pennington, 1981), while the subducting slab dips about 5° to the east and northeast between 5°S and 14°S (Barazangi and Isacks, 1976). The slab between the Peruvian and Pampean segments (14°S–27°S) dips normally, about 30° to the east (Cahill and Isacks, 1992; Ramos, 1999). The subduction dips 30° to the east between 33°S and 36°S, and 40° further south (Ramos, 1999). Subandean foreland basins are located to the east of the Andean chain, such as the Marañon basin in the north and Chaco basin in the south (Ramos, 1999).

The Precambrian South American Platform is mainly composed of three exposed shields (Atlantic shield in the east, Guyana shield in the north and Guaporé shield in the center), and buried Precambrian basement beneath three large intracratonic basins (Amazonian basin in the north, Parnaíba basin in the northeast and Paraná basin in the south). The Atlantic shield comprises four structural provinces: São Francisco craton, Borborema, Tocantins and Mantiqueira foldbelt provinces (Goodwin, 1991). The Guyana and Guaporé shields, together with their buried extensions, form the Amazonian Craton, a large province composed of Archean to early Proterozoic basement with widespread mid-Proterozoic cover (Almeida and Hasui, 1984; Goodwin, 1991). The Amazonian craton can be divided into six geochronologic provinces (Cordani and Sato, 1999; Tassinari and Macambira, 1999). The four main provinces are: Central Amazonian (>2.3 Ga), Maroni-Itacaiúnas (2.2–1.95 Ga), Ventuari-Tapajós (1.95–1.8 Ga) and Rio Negro-Juruena (1.8–1.55 Ga), labeled with “A”, “B”, “C”, “D”, respectively, in Fig. 9c. The other two provinces, Rondonian-San Ignácio (1.5–1.3 Ga) and Sunsás (1.25–1.0 Ga) at the southwestern border of the craton, are too small to be shown here. A major boundary between the Amazonian craton and the eastern part of the platform, called TransBrasiliano Lineament (TBL in Fig. 1) played a major role in the final assemblage of Gondwana in Late Proterozoic/Early Paleozoic times (Almeida et al., 2000). The TransBrasiliano Lineament seems to be a megasuture defining the boundary of several different crustal domains to the NW, including the Amazonian craton, and to the SE, including mainly the São Francisco craton (Cordani and Sato, 1999).

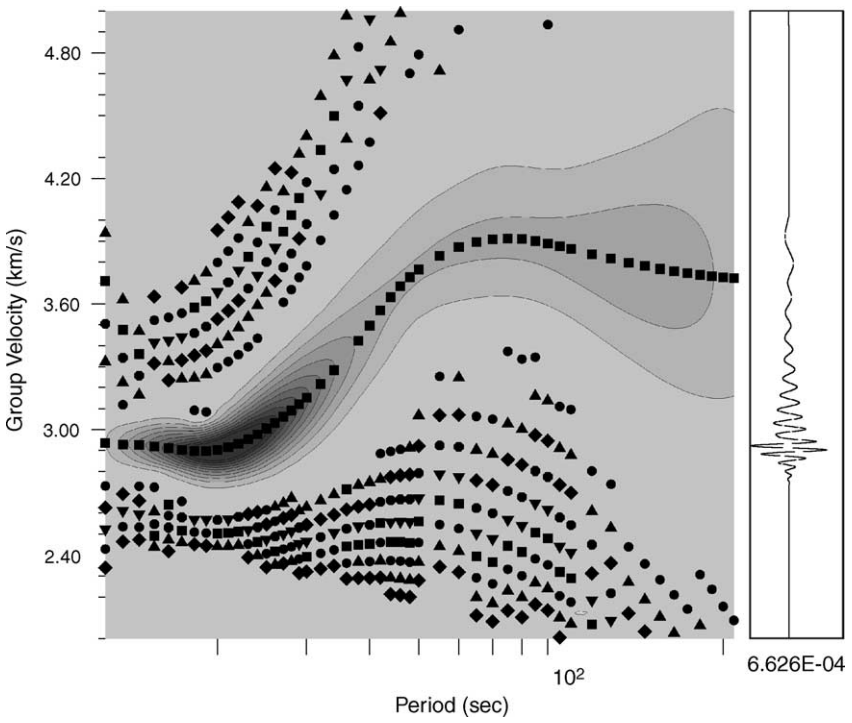

Fig. 3. An example of Rayleigh-wave dispersion processing with Multiple Filtering Technique (MFT). The left shows the amplitude spectrum of the multiple filtered seismogram. The right shows the phase-matched filtered seismogram used in the MFT. For each period, the black square in the center of the darkest contour is the maximum energy and represents a point in group-velocity dispersion. Other symbols are secondary peaks.

In the Late-Paleozoic Patagonian platform, a different basement is found dominated by numerous large Paleozoic granitoids with subordinate interspersed Precambrian, mainly mid to late Proterozoic terrains (Goodwin, 1991).

3. Data

Data from 1990 to 2003 recorded by portable stations installed in several projects (BLSP92, BLSP95 and BLSP02 since 1992) and by the permanent GSN stations were selected with emphasis on pure continental paths. More than 12,000 paths were examined and about 6000 Rayleigh- and 3500 Love-wave dispersion curves with good quality were retrieved. Fig. 2 shows the distribution of stations (triangles and squares) and earthquakes (circles) used for the Rayleigh and Love wave tomography at 30 s period. The newly installed stations (BLSP02 in Fig. 2) in northern Brazil were crucial for improving the path coverage in northern South America. In addition, the azimuthal path distribution in central Brazil was also improved.

Group velocities were determined using a Multiple Filtering Technique (MFT) (Dziewonski et al., 1969) with a phase-matched processing by MFT (Herrin and Goforth, 1977) to isolate the fundamental mode surface wave. We used a program by Herrmann and Ammon (2002) which uses the instantaneous frequency, taking into account the spectral amplitude variation (Nyman and Landisman, 1977) for each nominal frequency of analysis. Fig. 3 shows an example of Rayleigh wave processing by MFT with periods from 20 to 200 s. The period range of each dispersion curve depends on the magnitude of the earthquake and path length, longer periods from larger earthquakes being better recorded at longer distances. In this paper, we use the period range of 10–150 s for Rayleigh waves and 20–70 s for Love

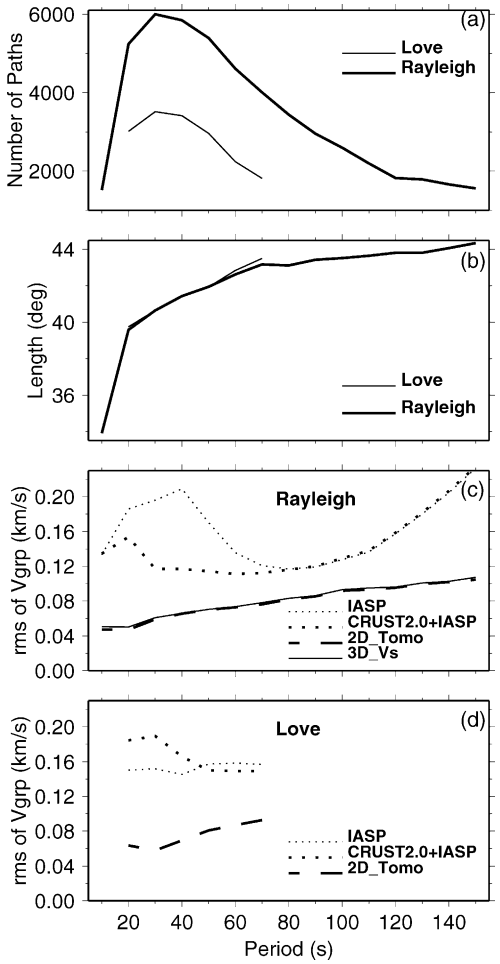

Fig. 4. Statistics of the data used in this study: (a) number of paths for each period of Rayleigh waves (thick line) and Love waves (thin line); (b) average path length, in degrees, of all paths for each period and wave type; (c) Rayleigh wave group-velocity deviations from the IASP model, the initial CRUST2.0 + IASP model, the 2D tomographic model, and the inverted 3D S-velocity model; (d) the same as (c), but for Love wave.

waves. The number of paths for each period is shown in Fig. 4a. The short periods (< 20 s) and long periods (>70 s) are measured for fewer paths than the intermediate periods (20–70 s). The average path length for each period is shown in Fig. 4b. The average path length of our data set (about 35°–45°) is significantly shorter than the data set used by Vdovin et al. (1999) (about 45°–75°), because they used many distant earthquakes and some stations outside the South American continent.

4. Group-velocity tomography

4.1. Inversion

As demonstrated in Section 5.2, our data set is capable of resolving features 400 km across laterally at crustal depths and 800 km across at 150 km. This is consistent with theoretical considerations based on widths of influence zones around the geometrical ray paths. Yoshizawa and Kennett (2002) showed that the geometrical ray method can be extended to sample an influence zone around the ray which is about one-third of the width of the first Fresnel zone. In our case, the average influence zone is about 2°–4° wide for periods of 20–100 s, respectively. For the maximum period of 150 s of our dataset, the influence zone is still wider (about 5°). This implies that the best possible resolution of our model varies from 300 km (crustal depth) to about 600 km (at lithospheric depths). Therefore, the studied region is gridded into 2° × 2° cells, and the group velocity for each grid cell was determined, by minimizing the following function:

$$\|As - t\|^2 + \lambda \|\Delta s\|^2$$

where A is the matrix of path segment length in each cell, s the slowness vector (inverse of group velocity), and t is the observed travel-time vector. Δs represents the first spatial gradient of the model, serving as smoothness for the final group-velocity maps; and λ is a weighting factor to balance between fitting the travel-times and smoothing the model. An appropriate factor λ was chosen for each period to produce smoothed group-velocity maps with lateral resolution compatible with the average width of the ray influence zones. The longer the period, the larger λ is chosen. The above equation was solved by a conjugate-gradient method, (LSQR of Paige and Saunders, 1982a,b) which is an efficient iterative method, especially for sparse and large linear systems, commonly applied in tomography (e.g., Nolet, 1990; Van der Lee and Nolet, 1997; Pasyanos et al., 2001; Marone et al., 2003).

The rms of the group-velocity residuals is one of the important factors to evaluate the final inverted tomographic model (Ritzwoller and Levshin, 1998; Vdovin

et al., 1999) and is given as:

$$\mathrm{rms} = \sqrt{\frac{1}{M}\sum_{i=1}^{M}(u_i^{\mathrm{obs}} - u_i^{\mathrm{pred}})^2}$$

where M is the number of paths for a given period and wave type, u_i^{obs} and u_i^{pred} are the observed and predicted group velocities for the ith path. The rms misfits of our 2D tomographic model for Rayleigh and Love waves are shown in Fig. 4c and d, respectively. The IASP curves (fine dotted lines) show the rms deviations between the observed group velocities and those given by the IASP global average model (Kennett and Engdahl, 1991). Laske et al. (2000) compiled a global model of crustal structure with $2^\circ \times 2^\circ$ grid based on the model CRUST5.1 (Mooney et al., 1998). In the continent, CRUST2.0 has two layers of sediments and three layers of crust with variable thicknesses. We combined the crustal sections of CRUST2.0 with the IASP upper mantle. In this combination, the two sedimentary layers and the upper crust of the CRUST2.0 model were averaged into a single layer to stabilize the 1D S-velocity inversions as we do not have enough information at short periods. The combined model, called CRUST2.0 + IASP, was used as initial model in our S-velocity inversion (see Section 5). The rms deviations between the observed group velocities and those from the CRUST2.0 + IASP are also shown in Fig. 4c and d. The CRUST2.0 + IASP in Fig. 4c fits our data better in the intermediate period range (20–70 s) than the uniform 35 km thick crust of the IASP model. The sedimentary section affects Love waves more than Rayleigh waves in the intermediate period range, so CRUST2.0 + IASP has a higher misfit than IASP for Love wave (Fig. 4d) because of the merging of the sedimentary layers with the upper crust. The dashed lines (2D_Tomo) show the fit of our inverted group-velocity model to the observed data. Our tomographic model produces an rms reduction relative to the CRUST2.0 + IASP model of about 50% on average for both Rayleigh and Love waves.

4.2. Group-velocity maps

We constructed group-velocity maps from 10 to 150 s for Rayleigh waves and from 20 to 70 s for Love waves by separate inversion in 10 s intervals. Maps of 20, 50 and 70 s periods for Rayleigh and Love wave are shown in Fig. 5. Group velocities are in percentage relative to the regional average of each period.

At short period (20 s), surface waves are sensitive to shallow crustal structure. In Fig. 5a, relatively low Rayleigh-wave group velocities are associated with all of the major sedimentary basins in South America, such as Amazonian, Parnaíba, Paraná and the subandean foreland basins. Love waves (Fig. 5b) only show low velocities in the Paraná basin which is the deepest of all the intracratonic basins, reaching 7 km depth (Milani and Zalán, 1999). The Parnaíba basin is less than 3.5 km thick and does not seem to affect Love waves significantly (Fig. 5b). The Amazonian basin has intermediate thicknesses and Love waves show average to low velocities at 20 s (Fig. 5b). Both Rayleigh and Love waves show low velocities in the Amazon Fan (depocenter at about 3°N, 49°W) which is up to 8 km thick (Driscoll and Karner, 1994). At longer period (50 s), surface waves become more sensitive to average crustal seismic velocity and crustal thickness. Lowest velocities are found along the whole Andean range, and generally high velocities in the platform (Fig. 5c,d), consistent with a thicker crust beneath the Andes. At 70 s, we are starting to sample the uppermost mantle. Higher velocities extend to the whole Amazonian craton and São Francisco craton (Fig. 5e,f).

Generally, our results are compatible in the large-scale features with those of Vdovin et al. (1999), whose lateral resolution ranges between 6° and 8°. Differences are found in the small-scale features. At 20 s, our group velocities correlate better with the large sedimentary basins, as shown in Fig. 5a,b. For example, the low velocity features along the east-west elongated Amazonian basin were imaged in our higher-resolution maps (Fig. 5a) but were not shown in the model of Vdovin et al. (1999). The use of short periods down to 10 s allowed imaging shallow structures, such as the sediment thicknesses.

5. Shear wave velocity

5.1. Inversion for S-velocity depth profiles

Because of the small period range (20–70 s) and fewer paths for Love waves (Fig. 4a), only the regionalized Rayleigh-wave dispersions were inverted for 1D

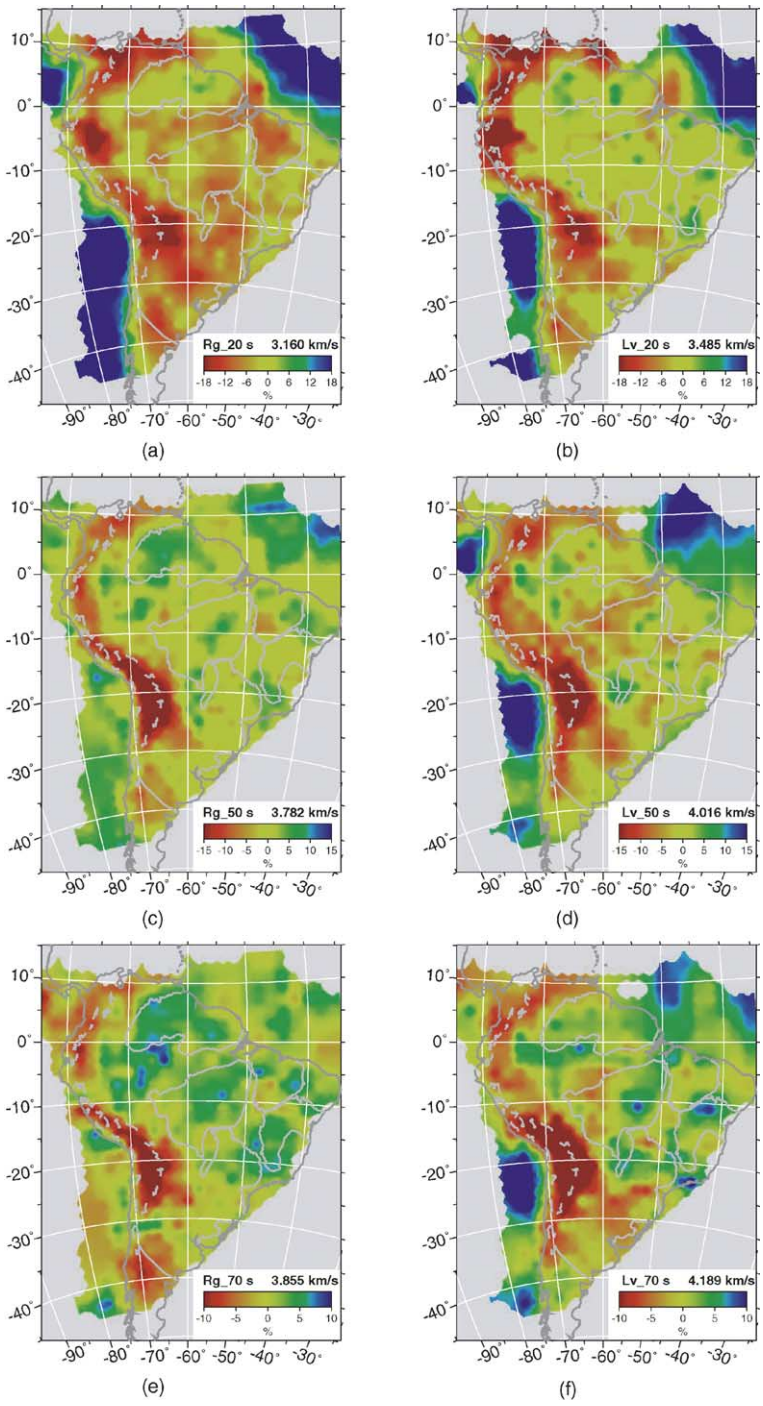

Fig. 5. Group-velocity tomographic maps at periods 20, 50 and 70 s for Rayleigh (Rg) and Love (Lv) waves.

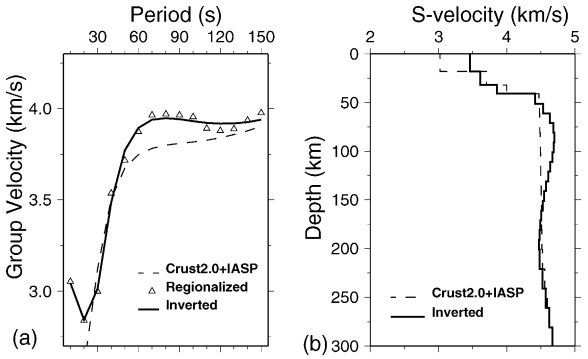

Fig. 6. Example of 1D velocity-depth inversion for a cell in the Paraná basin (21°S, 50°W). (a) The regionalized group velocities (triangles), dispersions calculated with the CRUST2.0 + IASP initial model (dashed line) and with the 1D S-velocity inverted model (solid line); (b) the initial CRUST2.0 + IASP model (dashed line) and the inverted S-velocity profile (solid line).

S-velocity depth profiles for all cells that comprise the final 3D S-velocity model. A linearized method (Herrmann and Ammon, 2002) was used in the 1D inversion with an initial velocity model consisting of horizontally homogeneous layers. Throughout the inversion, the thickness and V_p/V_s for each layer remained fixed and the density was estimated from the P-velocity. By iteratively perturbing the initial model, the final model is obtained when a good fit to the dispersion curve is achieved.

We set our starting model as CRUST2.0 + IASP, composed of the CRUST2.0 crustal structure overlying IASP91 upper mantle. Due to the decreasing resolution with depth, we used layers with 10 km thickness below the Moho down to 200 km depth, and 20 km thickness down to 400 km. S-velocities for depths deeper than 300 km are fixed during inversion since we have no resolution deeper than about 300 km for a maximum period of 150 s. To prevent large velocity oscillations between adjacent layers, smoothness constraint was applied in the inversion.

One example of 1D inverted S-velocity depth profile in the Paraná basin is shown in Fig. 6. The inverted model fits the regionalized dispersion much better than the initial CRUST2.0 + IASP model (dashed line). The slight oscillation of the regionalized dispersion for long periods (>110 s) is caused by larger uncertainties at longer periods.

Assembling the inverted 1D profiles of all cells, a final 3D S-velocity model was constructed. With this 3D model, the group velocity for each observed path was calculated and compared with the observed value. The rms difference between observed and calculated values is shown in Fig. 4c (solid line). Because Love-wave dispersion was not used in the S-velocity inversion, only the rms for Rayleigh wave was shown. The rms of the 3D model is very close to that of the 2D tomographic model, as expected.

5.2. Resolution test

To assess the spatially varying resolving power of our data, we did two types of resolution tests: regular checkerboard test and realistic structure test.

Several checkerboard tests were made, such as shown in Fig. 7, with S-velocity varying by ±7% relative to the IASP model for all depths. We calculated the group-velocity dispersion for all cells and synthetic travel-times for all observed paths. Random noises were added to the synthetic travel-times. The noise amplitude is equal to the average travel-time rms of all periods. The 2D tomography was carried out to obtain the regionalized dispersion for each cell (in $2^\circ \times 2^\circ$ grid), which was then inverted to obtain the 1D S-velocity profile. With these tests, we concluded that the central part of our model has resolution of about 4° at 30 km depth (Fig. 7a,b), resolution of 6° at 100 km (Fig. 7c,d) and 8° at 150 km (Fig. 7e,f). The resolution decreases near the margin of the study area. At 100 km depth, we can only interpret structures larger than about 650 km which is consistent with the geometrical ray approximation, given the width of the ray influence zones as discussed earlier.

In the realistic structure test, we give an input model with two profiles (geographical locations shown in Fig. 1): AA′ simulating the subduction of Nazca plate crossing the central Andes, and BB′ simulating the high and low velocity blocks across the Amazonian and São Francisco cratons. The input and retrieved structures of the two profiles are shown in Fig. 8a–d. The output model retrieved the general pattern of the input model down to about 200 km, which indicates the limit of the depth resolution of our dataset for continental scale structures.

5.3. 3D S-velocity model

The 3D S-velocity anomalies, relative to the IASP model, are shown in Fig. 9 for three depths (30,

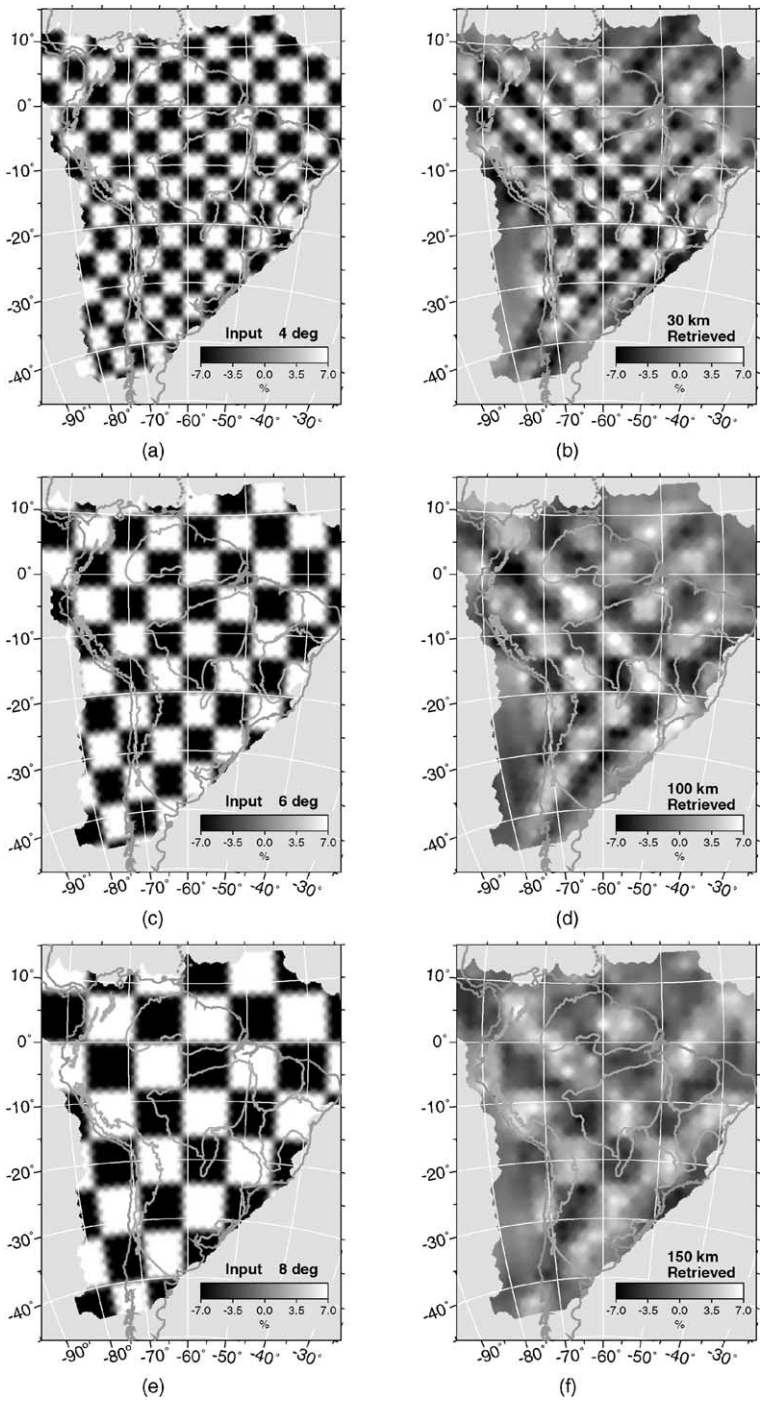

Fig. 7. Checkerboard test with input models (left column) of $4^\circ \times 4^\circ$ (a), $6^\circ \times 6^\circ$ (c) and $8^\circ \times 8^\circ$ checkers (e). Their retrieved model at 30 km (b), 100 km (d) and 150 km (f) are shown on the right column.

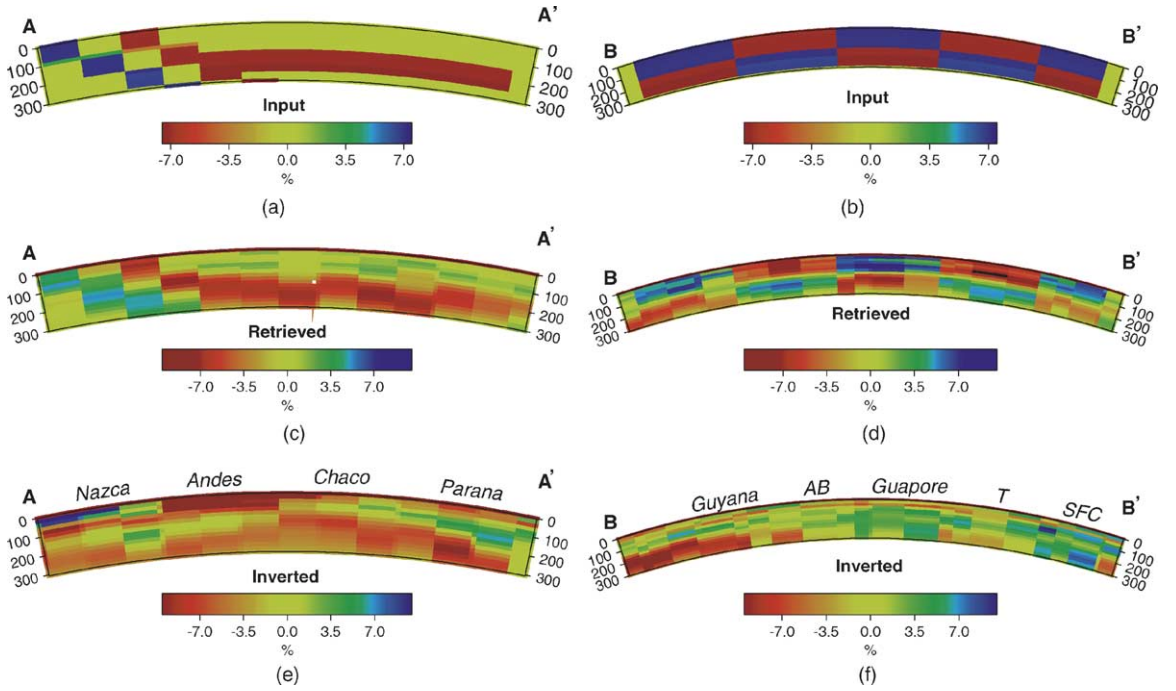

Fig. 8. Two vertical sections (AA′ and BB′) across our 3D model (e,f) and a resolution test (a–d). Their geographical positions are shown in Fig. 1. In the resolution test, (a) and (b) are the input models; (c) and (d) are the retrieved models. The labels in (e) and (f) represent the main geotectonic units crossed by the profiles, among which "AB" indicates the Amazonian basin, "T" denotes the Tocantins fold belt province near the TransBrasiliano Lineament, and "SFC" is the São Francisco craton.

100 and 150 km). The main features are discussed below.

(a) The 30 km map (Fig. 9a) shows the S-velocity distribution in the mid to lower continental crust (in the oceanic areas, upper mantle velocities at 30 km saturated the scale). Lowest velocities (down to −7%) were found beneath the highest elevation in the Andes (near 20°S, 68°W) where 30 km is in the middle crust. Such low velocities beneath the central Andes have been previously observed by Schmitz et al. (1999) and Yuan et al. (2000). Our map is in general agreement with the compilation of Christensen and Mooney (1995) which shows that, at 30 km depth, the average seismic velocity beneath orogens are 2% lower than the average velocity beneath shields. The large area of high velocities in the western Amazonian region (west of 70°W) and northern Bolivia is characterized by the highest Bouguer anomalies in South America, about 100 mGals higher than the rest of the stable platform (Sá et al., 1993; Chapin, 1996), but little is known about the crustal structure in this area to allow further interpretation. Relatively low velocities are found beneath the Paraná basin which are consistent with low velocities found by inversion of inter-station phase velocities in the central part of the basin (An and Assumpção, 2004). Slightly higher velocities are observed in the Pantanal basin compared to the surrounding areas. This feature is consistent with the positive Bouguer and free-air anomalies observed by Sá et al. (1993), Shiraiwa and Ussami (2001) and Woldemichael (2003), and interpreted as higher crustal density. An interesting feature of our model is the contrast between low velocities in the Paraná basin and high velocities in the southern part of the São Francisco craton and adjacent fold belts. A steep gravity gradient separates these two provinces (Lesquer et al., 1981; Ussami et al., 1993) but the

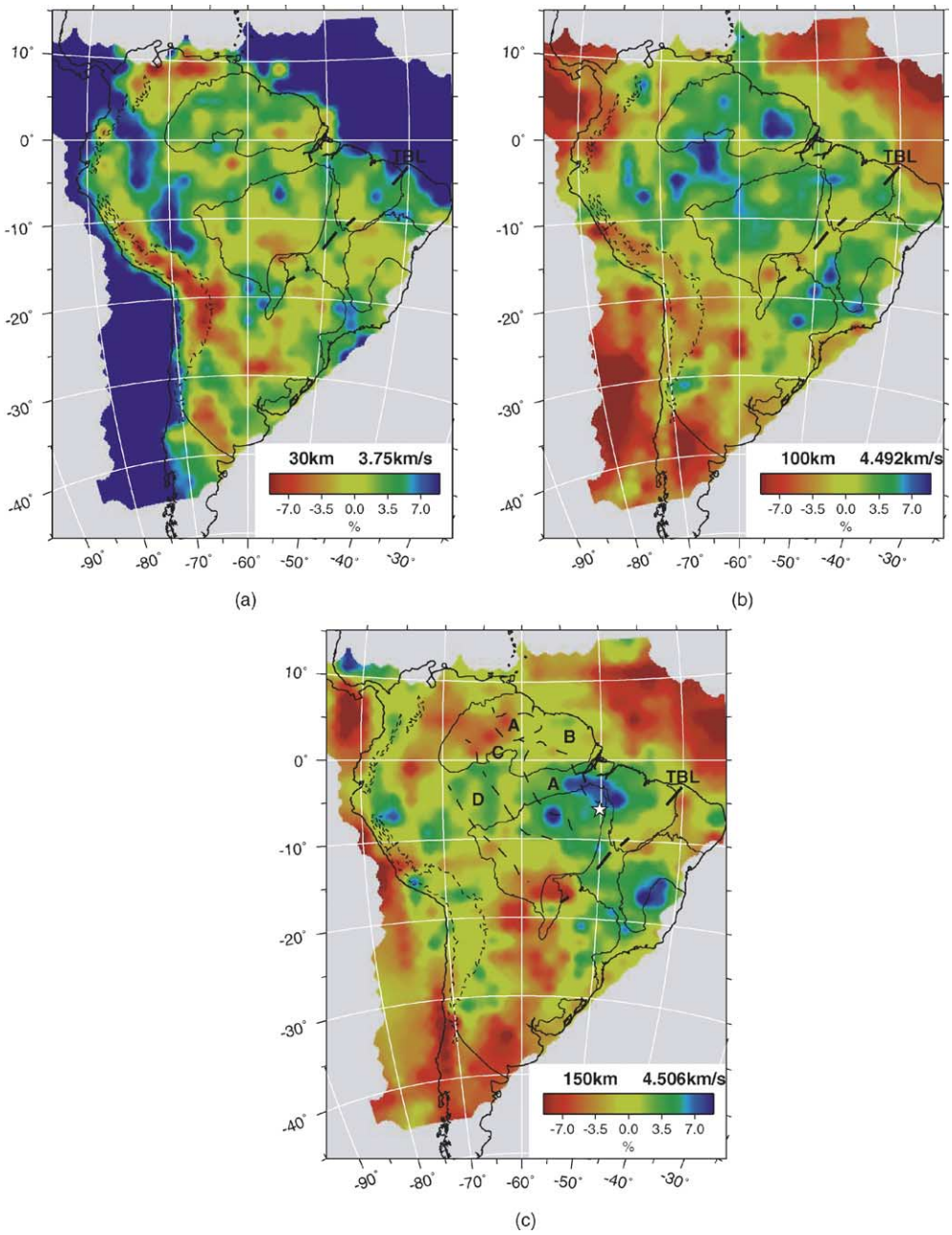

Fig. 9. Horizontal slices of the 3D S-velocity model at the depths of (a) 30 km, (b) 100 km, and (c) 150 km. The thick segmented line labeled "TBL" is the surface expression of the TransBrasiliano Lineament. The thin dashed lines labeled "A"–"D" in diagram (c) indicate the four main geochronologic provinces in the Amazonian craton: Central Amazonian ("A", >2.3 Ga), Maroni-Itacaiúnas ("B", 2.2–1.95 Ga), Ventuari-Tapajós ("C", 1.95–1.8 Ga) and Rio Negro-Juruena ("D", 1.8–1.55 Ga). The star in (c) indicates the location where the oldest Archean granitoids were found.

gravity-based suture model proposed by Lesquer et al. (1981) uses higher density beneath the Paraná basin. This apparent contradiction deserves further investigation.

(b) The Andean range is generally characterized by low velocity down to 100 km (Fig. 9b), probably due to the presence of wet asthenosphere near the subduction zone. Moreover, looking at the 100 km map, we find that the along-Andean low velocity anomalies are not continuous, but are broken near the three flat-slab segments by patches of average to high velocity. From north to south, the first break of the low velocity is in northern Colombia (8°N, 75°W) corresponding to the Bucaramanga flat-slab segment. The second break is in western Peru (from 5°S, 78°W to 9°S, 75°W), correlating with the Peruvian flat-slab segment. The third break is in central Chile (30°S, 69°W), corresponding to the Pampean flat-slab segment. This velocity pattern in the Andean region confirmed previous results from regional tomography (Van der Lee et al., 2001, 2002; Heintz, 2003), while global tomography (Shapiro and Ritzwoller, 2002; Ritzwoller et al., 2002) did not clearly resolve the flat-slab segments of the Nazca plate. The heat flow map of South America (Hamza and Muñoz, 1996) shows the same discontinuous feature. The Andean areas with strong low velocity anomalies have an average heat flow of 100 mW/m^2, while the parts with average to high velocities only have on average 50 mW/m^2 of heat flow (Hamza and Muñoz, 1996).

(c) General high upper mantle velocities were found in the whole Amazonian craton and the São Francisco craton down to 150 km (Fig. 9b,c). This large area of high velocity anomalies in the Precambrian cratons indicates a lithosphere at least 150 km thick. At 150 km (Fig. 9c), the high velocity anomalies seem to concentrate in a smaller area in the northeastern Guaporé shield (5°S, 50°W) and the southeastern São Francisco craton (15°S, 44°W). These high velocity anomalies at 150 km indicate a thicker lithosphere in these regions compared to other areas of the Precambrian cratons. A worldwide review of seismic structure showed that the lithosphere is thickest beneath Archean cratons and thinner beneath Proterozoic cratons (Durrheim and Mooney, 1994). Inside the Central Amazonian province, the oldest Archean granitoids (3.0–2.5 Ga) in South America were found at the Carajás metallogenic province (Sial et al., 1999), labeled with a star in Fig. 9c. The location of the oldest granitoids, is very close to the region with highest S-velocity anomaly in our model, consistent with the Durrheim and Mooney's compilation. The depth extent and amplitude of the high velocities in the western Amazonian craton are smaller than in the eastern part, indicating that the lithosphere in the west is thinner than in the east. This feature is in general agreement with the geochronologic provinces in the craton. The thinner part of the craton corresponds to the relatively younger Rio Negro-Juruena and Ventuari-Tapajos provinces in the west (1.55–1.95 Ga, "C" and "D" in Fig. 9c), and the thicker part corresponds to the older Central Amazonian and Maroni-Itacaiunas Provinces in the east (>1.95 Ga, "A" and "B" in Fig. 9c).

(d) Another interesting feature imaged by our model is a possible correlation with the TransBrasiliano Lineament (TBL in Fig. 9). Tracing from the NE coast of Brazil, through the Parnaíba basin and the Tocantins province into northern Paraguay, a NE–SW trending low velocity along TBL is found at upper mantle depths (see map of 100 km). High accuracy magnetic field anomalies from satellite and terrestrial aeromagnetic data over Brazil both imaged the TBL as a strong continental scale crustal feature (Fairhead and Maus, 2003). This feature is not observed in our lower crust map maybe due to the small geological contrast between the shear zone and the adjacent regions in addition to the limited lateral resolution of our model. However, the lineament seems characterized with low S velocities especially at 100 km, separating the high velocity/thick lithospheric domains to the NW and SE, which suggests that the TBL shear zone is not just a surface feature but is a zone with thinner lithosphere.

(e) Low S-velocities down to 150 km beneath the northern Pantanal basin (near 17°S, 57°W) and the Chaco basin has been consistently observed in several regional and global tomographic models (Van der Lee et al., 2001,2002; Shapiro and Ritzwoller, 2002; Ritzwoller et al., 2002; Heintz, 2003), suggesting that it is a major upper man-

tle feature beneath South America. Low velocities have also been mapped beneath the Pantanal basin by teleseismic P-wave tomography (Assumpção et al., 2004). Their model at 100 km depth is compared to our S-velocity model in SE Brazil in Fig. 10. Despite the difference raised by different lateral resolutions, our S-velocity model shows similar features to the P-wave model, such as the low velocities along the TBL, the general high velocities in the São Francisco craton and the eastern Paraná basin.

(f) The Patagonian platform located in the southern tip of the South American continent showed a different character from the Precambrian South American platform: strong low lithospheric velocities appeared in all depths. The Patagonian basement is dominated by Paleozoic granitoids, while the South American platform is mainly composed of Archean and early Proterozoic basement (Goodwin, 1991). A younger Patagonian basement seems consistent with such low lithospheric velocities. This feature was also seen in previous tomography (Vdovin et al., 1999; Shapiro and Ritzwoller, 2002; Ritzwoller et al., 2002; Heintz, 2003). However, our resolution in this part of South America is very limited (Fig. 7b,d,f).

To better view our 3D model, two representative cross sections (AA′ and BB′) are sliced and shown in Fig. 8e and f. The profile AA′ (geographical location shown in Fig. 1) starts in the Pacific Ocean, crosses the central Andes, the foreland Chaco basin, and ends in the intracratonic Paraná basin. Profile AA′ in the realistic structure test (Fig. 8a, c) is reasonably resolved down to 200 km. In our inverted model, this section (Fig. 8e) shows high velocity in thin lithosphere beneath the Nazca plate. The subducting Nazca slab is suggested but is not very clear. The Andes shows low velocities down to 100 km, and the subandean Chaco basin shows low velocities deeper in the asthenosphere. The intracratonic Paraná basin is characterized by low velocity in the crust and high velocity in the lithospheric upper mantle. The other section BB′ starts from the Amazonian craton, crosses the Tocantins province (composed mainly of fold belts), and ends in the São Francisco craton. The inverted model (Fig. 8f) shows that the lithosphere beneath the Guyana shield is thinner than beneath the Guaporé shield, confirming the

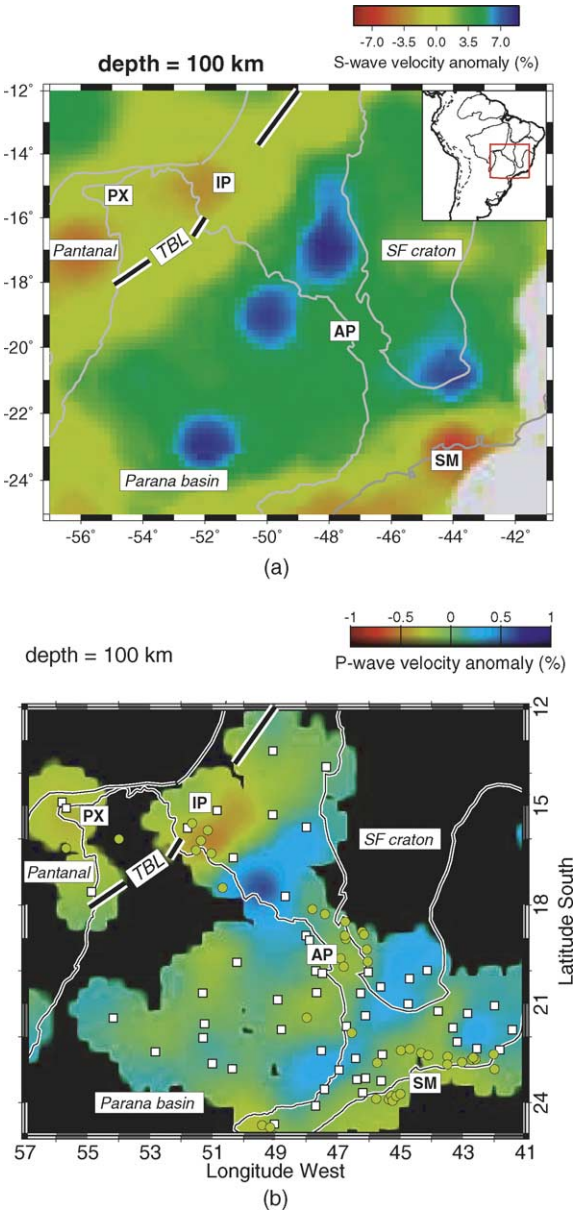

Fig. 10. Comparison of our S-velocity model in SE Brazil at 100 km with the P-wave velocity model of Assumpção et al. (2004).

observations of Heintz (2003). Between the Guaporé shield and the São Francisco craton (SFC), a low velocity belt was imaged, corresponding to the Tocantins fold belt province (T) near the TransBrasiliano Lineament.

6. Conclusions

Newly installed stations in northern Brazil improved the path coverage in northern South America, permitting us to image the lithosphere of South America with better resolution, especially in the Amazonian region (northern and northeastern Brazil), an area not studied with enough resolution in previous tomography. Using recordings from old BLSP and GSN stations and new portable BLSP02 stations, we determined 2D group-velocity tomographic maps for both Rayleigh and Love waves and an isotropic 3D lithospheric S-velocity model for the whole South American continent by inverting the regionalized Rayleigh-wave dispersions.

Our group-velocity maps show more detailed features besides confirming the features shown in previous large-scale group-velocity tomography. The large east-west elongated Amazonian sedimentary basin was well delineated by low velocities on our 20 s maps, but was not shown by Vdovin et al. (1999).

Our 3D S-velocity model showed good correlation with the main geological units and with the large scale patterns of heat flow in the Andes. The good correlation with the flat-slab segments in the Andes at 100 km depth shows that our ray-theory based tomography can retrieve structures at the scale of a few hundred kilometers. The 3D model confirmed both the regional features of SE Brazil and the continental-scale features of central and western South America in previous studies, such as the deep low velocity anomaly beneath the Chaco basin and the high lithospheric velocity in the stable South American platform. Furthermore, new features were imaged by our 3D S-velocity model. The TransBrasiliano Lineament seems to follow a belt of low velocities at lithospheric depth, confirming its importance as a boundary between different lithospheric provinces. A 150 km depth extent of high S-velocity beneath the eastern Amazonian craton implies its lithosphere is thicker than beneath the western Amazonian craton, where high velocity extends to ∼100 km. High S-velocity concentration at 150 km were found in the areas of Archean nuclei located in the eastern Amazonian craton and southeastern São Francisco craton.

Acknowledgments

Project financed mainly by MCT Mineral Fund, Brazil, and ETH-Z, Switzerland (grant 0-20990-02), with additional support from FAPESP (grants 96/01566-0, 01/06066-6, 02/00244-2), and CNPq (30.0227/79, 52.0078/00-4). We greatly appreciate the generosity of ETH-Z professors Domenico Giardini and Eduard Kissling in loaning us ten sets of their broadband seismic equipment for this project. We are grateful to Federica Marone for comments on a previous version of this manuscript. We thank Federica Marone, Mark Van der Meijde, Peter Zweifel, Beat Rinderknecht, Andre Blanchard, Eduardo Mandel, José Roberto Barbosa and Marcelo Bianchi for fieldwork and general support. We thank Robert B. Herrmann for sharing the surface wave processing and inversion programs, and Meijian An for helping with computational problems.

References

Almeida, F.F.M., Hasui, Y., 1984. O Pré-cambriano do Brasil. Edgard Blücher, São Paulo, Brazil.

Almeida, F.F.M., Neves, B.B.B., Carneiro, C.D.R., 2000. The origin and evolution of the South American Platform. Earth-Sci. Rev. 50, 77–111.

Alsina, D., Woodward, R.L., Snieder, R.K., 1996. Shear velocity structure in North America from large-scale waveform inversion of surface waves. J. Geophys. Res. 101 (B7), 15969–15986.

An, M., Assumpção, M.S., 2004. Multi-objective inversion of surface waves and receiver functions by competent genetic algorithm applied to the crustal structure of the Paraná Basin, SE Brazil. Geophys. Res. Lett. 31 (5), L05615, doi:10.1029/2003GL019179.

Assumpção, M.S., Schimmel, M., Escalante, C., Barbosa, J.R., Rocha, M., Barros, L.V., 2004. Intraplate seismicity in SE Brazil: stress concentration in lithospheric thin spots. Geophys. J. Int. 159, 390–399.

Barazangi, M., Isacks, B., 1976. Spatial distribution of earthquakes and subduction of the Nazca plate beneath South America. Geology 4, 686–692.

Boschi, L., Ekstrom, G., 2002. New images of the Earth's upper mantle from measurement of surface-wave phase velocity anomalies. J. Geophys. Res. 107 (B4), doi:10.1029/2000JB000059.

Cahill, T., Isacks, B.L., 1992. Seismicity and the shape of the subducted Nazca plate. J. Geophys. Res. 97 (B12), 17503–17529.

Chapin, D.A., 1996. A deterministic approach toward isostatic gravity residuals – a case study from South America. Geophysics 61 (4), 1022–1033.

Christensen, N.I., Mooney, W.D., 1995. Seismic velocity structure and composition of the continental crust: a global view. J. Geophys. Res. 100 (B6), 9761–9788.

Cordani, U.G., Sato, K., 1999. Crustal evolution of the South American Platform, based on Nd isotopic systematics on granitoid rocks. Episodes 22 (3), 167–173.

Debayle, E., Kennett, B.L.N., 2000. The Australian continental upper mantle: Structure and deformation inferred from surface waves. J. Geophys. Res. 105 (B11), 25423–25450.

Dorbath, C., Masson, F., 2000. Composition of the crust and upper-mantle in the central Andes (19°30′S) inferred from P velocity and Poisson's ration. Tectonophysics 327, 213–223.

Driscoll, N.W., Karner, G.D., 1994. Flexural deformation due to Amazon Fan loading: a feedback mechanism affecting sediment delivery to margins. Geology 22, 1015–1018.

Durrheim, R.J., Mooney, W.D., 1994. Evolution of the Precambrian lithosphere: Seismological and geochemical constraints. J. Geophys. Res. 99 (B8), 15359–15374.

Dziewonski, A., Block, S., Landisman, M., 1969. A technique for the analysis of transient seismic signals. Bull. Seism. Soc. Am. 59, 427–444.

Ekstrom, G., Dziewonski, M., 1998. The unique anisotropy of the Pacific upper mantle. Nature 394, 168–172.

Engdahl, E.R., Van der Hilst, R.D., Berrocal, J., 1995. Imaging of subducted lithosphere beneath South America. Geophys. Res. Lett. 22 (16), 2317–2320.

Fairhead, J.D., Maus, S., 2003. CHAMP satellite and terrestrial magnetic data help define the tectonic model for South America and resolve the lingering problem of the pre-break-up fit of the South Atlantic Ocean. Lead. Edge 22 (8), 779–783.

Godey, S., Snieder, R., Villaseñor, A., Benz, H.M., 2003. Surface wave tomography of North America and the Caribean using global and regional broad-band networks: phase velocity maps and limitations of ray theory. Geophys. J. Int. 152, 620–632.

Goodwin, A.M., 1991. Precambrian Geology. Academic Press.

Grand, S.P., 1994. Mantle shear structure beneath the Americas and surrounding oceans. J. Geophys. Res. 99 (B6), 11591–11622.

Haberland, C., Rietbrock, A., 2001. Attenuation tomography in the western central Andes: A detailed insight into the structure of a magmatic arc. J. Geophys. Res. 106 (B6), 11151–11167.

Hamza, V.M., Muñoz, M., 1996. Heat flow map of South America. Geothermics 25 (6), 599–646.

Heintz, M., 2003. Structure et Déformation du Manteau Continental Sud Américain: Apport de la Tomographie en Ondes de Surface et de L'anisotropie Sismique. PhD. Thesis, ISTEEM, University of Montpellier II, France, http://rses.anu.edu.au/∼maggy/these.html.

Heintz, M., Debayle, E., Vauchez, A., 2004. Upper mantle structure of the South American continent and neighboring oceans from surface wave tomography. Tectonophysics, submitted for publication.

Herrin, E., Goforth, T., 1977. Phase-matched filters: Application to the study of Rayleigh waves. Bull. Seism. Soc. Am. 67, 1259–1275.

Herrmann, R.B., Ammon, C.J., 2002. Computer Programs in Seismology – Surface Waves, Receiver Functions and Crustal Structure. Saint Louis University, http://www.eas.slu.edu/People/RBHerrmann/ComputerPrograms.html.

Huang, Z., Su, W., Peng, Y., Zheng, Y., Li, H., 2003. Rayleigh wave tomography of China and adjacent regions. J. Geophys. Res. 108 (B2), 2073, doi:10.1029/2001JB001696.

Kennett, B.L.N., Engdahl, E.R., 1991. Traveltimes for global earthquake location and phase identification. Geophys. J. Int. 105, 429–465.

Larson, E.W.F., Ekstrom, G., 2001. Global models of surface wave group velocity. Pure Appl. Geophys. 158, 1377–1399.

Laske, G., Masters, G., Reif, C., 2000. CRUST2.0: A new global crustal model at 2° × 2°. http://mahi.ucsd.edu/Gabi/rem.html.

Lesquer, A., Almeida, F.F.M., Davino, A., Lachaud, J.C., Maillard, P., 1981. Signification structurales des anomalies gravimetriques de la partie sud du craton de S. Francisco (Brésil). Tectonophysics 76, 273–293.

Marone, F., Van der Meijde, M., Van der Lee, S., Giardini, D., 2003. Joint inversion of local, regional and teleseismic data for crustal thickness in the Eurasia-Africa plate boundary region. Geophys. J. Int. 154, 499–514.

Milani, E.J., Zalán, P.V., 1999. An outline of the geology and petroleum systems of the Paleozoic interior basins of South America. Episodes 22 (3), 199–205.

Mooney, W.D., Laske, G., Masters, G., 1998. CRUST 5.1: A global crustal model at 5° × 5°. J. Geophys. Res. 103 (B1), 727–747.

Myers, S.C., Beck, S., Zandt, G., Wallace, T., 1998. Lithospheric-scale structure across the Bolivian Andes from tomographic images of velocity and attenuation for P and S wave. J. Geophys. Res. 103 (B9), 21233–21252.

Nettles, M., Dziewonski, A., 2003. Tomographic modeling of the North American upper mantle. Eos Trans. AGU 84 (46). Fall Meet. Suppl., Abstract S32E-05.

Nolet, G., 1990. Partitioned waveform inversion and two-dimensional structure under the Network of Autonomous Recording Seismographs. J. Geophys. Res. 95 (B6), 8499–8512.

Nolet, G., Dahlen, F.A., 2000. Wave front healing and the evolution of seismic delay times. J. Geophys. Res. 105 (B8), 19043–19054.

Nyman, D.C., Landisman, M., 1977. The display equalized filter for frequency-time analysis. Bull. Seism. Soc. Am. 67, 393–404.

Paige, C.C., Saunders, M.A., 1982a. LSQR: An algorithm for sparse linear equations and sparse least squares. ACM TOMS 8, 43–71.

Paige, C.C., Saunders, M.A., 1982b. Algorithm 583, LSQR: Sparse linear equations and least-squares problems. ACM TOMS 8, 195–209.

Pasyanos, M.E., Walter, W.R., Hazler, S.E., 2001. A surface wave dispersion study of the Middle East and North Africa for monitoring the Comprehensive Nuclear-Test-Ban Treaty. Pure Appl. Geophys. 158, 1445–1474.

Pennington, W.D., 1981. Subduction of the eastern Panama basin and seismotectonics of northwest South America. J. Geophys. Res. 86, 10753–10770.

Ramos, V.A., 1999. Plate tectonic settings of the Andean Cordillera. Episodes 22 (3), 183–190.

Ritzwoller, M.H., Shapiro, N.M., Barmin, M.P., Levshin, A.L., 2002. Global surface wave diffraction tomography. J. Geophys. Res. 107 (B12), 2335, doi:10.1029/2002JB001777.

Ritzwoller, M.H., Levshin, A.L., 1998. Eurasian surface wave tomography: group velocities. J. Geophys. Res. 103 (B3), 4839–4878.

Sá, N.G., Ussami, N., Molina, E.C., 1993. Gravity map of Brazil 1: representation of free-air and Bouguer anomalies. J. Geophy. Res. 98 (B2), 2187–2197.

Schimmel, M., Assumpção, M., VanDecar, J.C., 2003. Seismic velocity anomalies beneath SE Brazil from P and S wave travel time inversions. J. Geophys. Res. 108 (B4), 2191, doi:10.1029/2001JB000187.

Schmitz, M., Lessel, K., Giese, P., Wigger, P., Araneda, M., Bribach, J., Graeber, F., Grunewald, S., Haberland, C., Lüth, S., Röwer, P., Ryberg, T., Schulze, A., 1999. The crustal structure beneath the Central Andean forearc and magmatic arc as derived from seismic studies – the PISCO 94 experiment in northern Chile (21°S–23°S). J. South Am. Earth Sci. 12, 237–260.

Shapiro, N.M., Ritzwoller, M.H., 2002. Monte-Carlo inversion for a global shear-velocity model of the crust and upper mantle. Geophys. J. Int. 151, 88–105.

Shiraiwa, S., Ussami, N., 2001. Gravity survey of the Pantanal wetland: data acquisition and processing. Rev. Bras. Geofísica 19 (3), 315–323.

Sial, A.N., Agnol, R.D., Ferreira, V.P., Nardi, L.V.S., Pimentel, M.M., Wiedemann, C.M., 1999. Precambrian granitic magmatism in Brazil. Episodes 22 (3), 191–198.

Silveira, G., Stutzmann, E., 2002. Anisotropic tomography of the Atlantic ocean. Phys. Earth Planet. Inter. 132, 237–248.

Silveira, G., Stutzmann, E., Griot, D., Montagner, J., Victor, L.M., 1998. Anisotropic tomography of the Atlantic ocean from Rayleigh surface waves. Phys. Earth Planet. Inter. 106, 257–273.

Simons, F.J., Zielhuis, A., Van der Hilst, R.D., 1999. The deep structure of the Australian continent from surface wave tomography. Lithos 48, 17–43.

Snieder, R., 1988. Large-scale waveform inversion of surface waves for lateral heterogeneity, 2, Application to surface waves in Europe and the Mediterranean. J. Geophys. Res. 93 (B10), 12067–12080.

Snoke, J.A., James, D., 1997. Lithospheric structure of the Chaco and Paraná basins of South America from surface-wave dispersion. J. Geophys. Res. 102 (B2), 2939–2951.

Snoke, J.A., Sambridge, M., 2002. Constraints on the S wave velocity structure in a continental shield from surface wave data: Comparing linearized least squares inversion and the direct search Neighbourhood Algorithm. J. Geophys. Res. 107 (B5), doi:10.1029/2001JB000498.

Souza, J.L., 1991. Crustal and upper mantle structures of the Brazilian coast. Pure Appl. Geophys. 136, 245–264.

Spetzler, J., Trampert, J., Snieder, R., 2002. The effect of scattering in surface wave tomography. Geophys. J. Int. 149, 755–767.

Tassinari, C.C.G., Macambira, M.J.B., 1999. Geochronological provinces of the Amazonian Craton. Episodes 22 (3), 174–182.

Ussami, N., Sá, N.C., Molina, E.C., 1993. Gravity map of Brazil II: regional and residual isostatic anomalies and their correlation with major tectonic province. J. Geophys. Res. 98 (B2), 2199–2208.

Van der Lee, S., Nolet, G., 1997. Uppermantle Svelocity structure of North America. J. Geophys. Res. 102 (B10), 22815–22838.

Van der Lee, S., James, D., Silver, P., 2001. Upper mantle S velocity structure of central and western South America. J. Geophys. Res. 106 (B12), 30821–30834.

Van der Lee, S., James, D., Silver, P., 2002. Correction to "Upper mantle S velocity structure of central and western South America," by Suzan Van der Lee, David James, and Paul Silver. J. Geophys. Res. 107 (B5), 2099.

VanDecar, J.C., James, D.E., Assumpção, M., 1995. Seismic evidence for a fossil mantle plume beneath South America and implications for plate driving forces. Nature 378, 25–31.

Vdovin, O., Rial, J.A., Levshin, A.L., Ritzwoller, M.H., 1999. Group-velocity tomography of South America and the surrounding oceans. Geophys. J. Int. 136, 324–340.

Villaseñor, A., Ritzwoller, M.H., Levshin, A.L., Barmin, M.P., Engdahl, E.R., Spakman, W., Trampert, J., 2001. Shear velocity structure of central Eurasia from inversion of surface wave velocities. Phys. Earth Planet. Inter. 123, 169–184.

Vuan, A., Russi, M., Panza, G.F., 2000. Group velocity tomography in the subantarctic Scotia sea region. Pure Appl. Geophys. 157, 1337–1357.

Woldemichael, S.F., 2003. Estruturas Geoelétricas Crustais da Bacia do Pantanal e Faixa Paraguai: Implicações Tectônicas. PhD. thesis, IAG-University of São Paulo, Brazil.

Yanovskaya, T.B., Kozhevnikov, V.M., 2003. 3D S-wave velocity pattern in the upper mantle beneath the continent of Asia from Rayleigh wave data. Phys. Earth Planet. Inter. 138, 263–278.

Yoshizawa, K., Kennett, B.L.N., 2002. Determination of the influence zone for surface wave paths. Geophys. J. Int. 149, 444–453.

Yuan, X., Sobolev, S.V., Kind, R., Oncken, O., Bock, G., Asch, G., Schurr, B., Graeber, G., Rudloff, A., Hanka, W., Wylegalla, K., Tibi, R., Haberland, Ch., Rietbrock, A., Giese, P., Wigger, P., Röwer, P., Zandt, G., Beck, S., Wallace, T., Pardo, M., Comte, D., 2000. Subduction and collision processes in the Central Andes constrained by converted seismic phases. Nature 408, 958–961.

Zielhuis, A., Nolet, G., 1994. Shear-wave velocity variations in the upper mantle beneath central Europe. Geophys J. Int. 117, 695–715.